RSC Advances

ROYAL SOCIETY OF CHEMISTRY

PAPER

View Article Online
View Journal | View Issue

Cite this: *RSC Adv.*, 2026, **16**, 14439

Coupling laboratory FTIR data with PROCODA kinetic modeling for the radiolysis of frozen formic acid using swift ions

L. Moraes, * C. M. Fargnoli and S. Pilling

Formic acid (HCOOH) is one of the simplest carboxylic acids detected in interstellar and circumstellar environments, often associated with prebiotic organic chemistry. In this work, we combine laboratory data from the radiolysis of pure HCOOH ice at 15 K by 267 MeV $^{56}Fe^{22+}$ ions with kinetic simulations performed using the PROCODA code. This numerical model solves a system of coupled differential equations describing 1631 reactions among 73 molecular and radical species, allowing the determination of effective reaction rate coefficients (ERCs), equilibrium abundances, and desorption yields. The best-fit model successfully reproduces experimental infrared data and predicts the formation of non-observed intermediates such as HOCO, CH_2OO, and H_2CO. The results indicate that CO, CO_2, and H_2O are the dominant radiolysis products, while HCOOH acts primarily as a transient radical source rather than a net precursor of complex organics. Hydrogen abstraction and radical recombination were identified as the main mechanisms governing molecular evolution, with HOCO and OH radicals playing key intermediate roles. The calculated desorption yield (1.5×10^5 molecules per ion) and effective rate constants confirm the efficiency of heavy ion sputtering in cold ices. These findings provide quantitative insight into the radiation-driven chemistry of formic acid and offer constraints for astrochemical models of dense clouds, protostellar disks, and icy moons.

Received 10th December 2025
Accepted 15th February 2026

DOI: 10.1039/d5ra09577h

rsc.li/rsc-advances

1. Introduction

Formic acid (HCOOH) is one of the simplest carboxylic acids detected in various environments, including astrophysical ones, and is of significant interest to astrochemistry. It has been identified in a variety of cold regions, such as protostellar ices, comets, and dense molecular clouds, as well as in warmer star-forming regions like Sgr B2, Orion KL, and W51.[1,2] In these environments, HCOOH is often found in association with other complex organic molecules, such as methylamine and acetic acid, and is considered a potential precursor to glycine.[2] At low temperatures, such as those studied by Andrade *et al.*[3] (2013), this ice is commonly found in space within regions shielded from direct stellar ultraviolet radiation such as icy grain mantles in dense clouds and protoplanetary disks—where the chemical processing is dominated by ionizing agents, mainly cosmic rays and X-rays. Under these conditions, energetic irradiation can induce bond cleavage and radical formation in the solid phase, triggering reaction pathways that lead to the synthesis of more complex species.

To simulate this space chemistry in the laboratory, Andrade *et al.*[3] (2013) condensed pure HCOOH vapor on a cold substrate 15 K and irradiated it with 267 MeV $^{56}Fe^{22+}$ ions (a heavy, highly charged cosmic-ray analogue).[3] *In situ* Fourier-transform infrared (FTIR) spectroscopy (4000–600 cm^{-1}) was used to monitor the ice composition during irradiation.[3] These experiments determined the destruction cross section of HCOOH and the formation cross sections of the daughter species. The dominant products identified in the ice were CO, CO_2 and H_2O, and from the fitted decay rates Andrade *et al.* inferred an effective HCOOH half-life of order 10^8 years under cosmic-ray flux in dense clouds.[3] Sputtering yields and complementary mass-spectrometry data were also reported in that study. These results establish a quantitative baseline for HCOOH radiolysis in astrophysical ices.

Previous laboratory studies have approached HCOOH processing by other ionizing sources. For example, Andrade *et al.*[3] (2013) investigated soft X-ray photolysis of HCOOH ice (at ~56 K) and used a ^{252}Cf fission-fragment source; both yielded outcomes broadly like those from ion-beam experiments 3. Notably, Andrade *et al.* found that most ionic fragments produced by X-rays also appear under energetic ion bombardment, but some species (*e.g.* the $HCOO^-/COOH^-$ anion) are only observed in heavy ion radiolysis.[3] Likewise, Pilling *et al.*[2] (2006) and collaborators used vacuum-UV and soft X-ray beams on HCOOH and related carboxylic acids, measuring fragment ions and cross sections under conditions relevant to star-forming regions.[2,3] These complementary experiments (using

Universidade do Vale do Paraiba -UNIVAP, Av. Shishima Hifumi, 2911, São Jose dos Campos, SP, Brazil. E-mail: leonardomoraes580@gmail.com; carolinemilena499@gmail.com; sergiopilling@yahoo.com.br

synchrotrons and cosmic-ray analog sources) all employed low-temperature ice analogs and advanced spectroscopic detection, providing a methodological framework and reference data for our kinetic modeling.

Over the years, the PROCODA code has been extensively applied to model and map the chemical evolution of astrophysical ices under different irradiation sources and cryogenic temperatures. Applications to pure ices include studies of CO_2,[4,5] CO,[6,7] H_2O,[8,9] CH_4,[10,11] and CH_3CN.[12,13] The code has also been successfully employed to investigate the chemical evolution of binary ice systems such as $H_2O:N_2$,[14] $H_2O:O_2$,[15,16] $H_2O:CO_2$,[17] $H_2O:HCOOH$,[18] and $CO:CO_2$.[19] In addition, forthcoming articles will address the chemical evolution of irradiated mixed ices containing $H_2O:CO$ and $H_2O:CH_4$, which are currently in preparation.

Despite the wealth of experimental measurements, infrared spectroscopy cannot directly detect many intermediate radicals or transient ions. The recorded IR bands quantify only the stable neutral products (CO, CO_2, H_2O, *etc.*), and overlapping features or band strength uncertainties may obscure less abundant species. Hence, the underlying reaction network (formation of radicals, ions and short-lived intermediates) remains partly hidden. To address this, we use a computational kinetic model that solves a system of coupled ordinary differential equations for a proposed reaction network. In this way we can simulate the time-dependent abundances of all species (observed and "hidden") during radiolysis. This approach is analogous to the PROCODA modeling recently applied by Pilling and co-workers to CO_2 ice processing.[3] In that work, a network of tens of reactions (direct dissociations, radical–radical recombination, *etc.*) was fit to experimental data, yielding reaction rates and concentrations of non-observed species.[3] Similarly, by fitting our kinetic model to the Andrade *et al.*[3] (2013) HCOOH data, we aim to infer plausible reaction pathways and estimate intermediate concentrations that were not accessible from the IR spectra alone.

This article addresses the chemical evolution of HCOOH ice at 15 K under cosmic ray irradiation, modeled with the PROCODA code. We reanalyzed the experimental data originally reported by Andrade *et al.*[3] (2013), which identified and quantified only four molecular species, and extended the chemical mapping to a total of 73 species formed during the irradiation process, comprising the four experimentally observed molecules plus 69 additional species expected to exist within the ice. These additional species were considered from Several laboratory and observational studies that have investigated the chemistry of formic acid in space.

The current model incorporates a network of 1631 coupled chemical reactions, accounting for processes such as radiation-induced dissociation, bimolecular reactions, and desorption. From this, we computed effective reaction rate coefficients (ERCs), characterized molecular abundances at chemical equilibrium (under high radiation fluence), and quantified radiation-induced desorption. Among the identified products are several prebiotically relevant organics, we discuss key reaction mechanisms responsible for their formation within the ice. As discussed, previously,[6] it is important to distinguish between the "effective" rate coefficient (ERC) used here and the traditional "ordinary" rate constant (k) from gas-phase chemistry. The ERC captures how reactants in the ice interact with constantly changing neighbors under varying density and temperature conditions, influenced by radiation. As such, it represents a time- and space-averaged rate over the course of irradiation, offering a more realistic description of ice processes. To improve modeling accuracy, astrochemical ice models should employ ERCs rather than gas-phase rate constants, accounting for the inherently heterogeneous and evolving nature of irradiated ices.

Finally, we note that while 15 K formic acid ice under 267 MeV, Fe bombardment is an extreme environment not found on Earth, the fundamental chemistry is governed by universal physics. Energy deposition by ionizing radiation, bond cleavage and radical recombination are central themes in radiation chemistry and condensed-phase kinetics generally. Thus, the reaction mechanisms and rate-equation modeling employed here have broader relevance to physical chemistry; insights gained may inform understanding of analogous processes (*e.g.* radiation damage, low-temperature catalysis) under terrestrial conditions.

2. Methodology

In this section, we describe the experimental data used in this study, including the data acquisition and processing procedures, as well as the computational modeling strategy. The experimental data set corresponds to the mid-infrared spectra of a pure HCOOH ice irradiated under astrophysical relevant conditions, originally reported by Andrade *et al.*[3] (2013). To simulate the chemical evolution of irradiated ices, we employed the PROCODA code, developed by Pilling *et al.*[4] (2022), which numerically determines the effective reaction rate coefficients, chemical abundances, and desorption parameters, fitting the model output to the experimental abundances.

2.1 The experimental data

This study revisits the chemical analysis of pure formic acid (HCOOH) previously conducted by Andrade *et al.*[3] (2013). In brief, gaseous formic acid was deposited onto a CSI substrate maintained at 15 K within an ultra-high vacuum chamber, forming a thin film approximately 2 microns thick. This film was irradiated with heavy ions ($^{56}Fe^{22+}$ at 267 MeV) at the Grand Accélérateur National d'Ions Lourds (GANIL) in Caen, France. *In situ* chemical characterization was carried out using a Fourier Transform Infrared (FTIR) spectrometer (Nicolet Magna 550), covering the spectral range from 4000 to 600 cm^{-1} with a resolution of 1 cm^{-1}. During the experiments, the chamber pressure remained below 2×10^{-8} mbar. Infrared spectra were acquired at various ion fluences, reaching up to 1×10^{13} ions cm^{-2}. The spectral analysis revealed that primary molecular products formed after irradiation were CO and CO_2, along with other more complex species that were not quantified. The authors monitored the chemical evolution of only four species during

ice irradiation: H_2O, HCOOH, CO and CO. Some experimental parameters are summarized in Table 1.

Fig. 1 presents infrared spectra and corresponding column-density evolution for pure HCOOH ice irradiated by 267 MeV Fe^{22+} ions at 15 K taken from Andrade *et al.*[3] (2013). Panel a shows the infrared absorbance spectra of HCOOH ice before and after irradiation by heavy ions, illustrating the spectral evolution resulting from radiolysis. After irradiation, new bands appear most notably those associated with the formation of CO, CO_2, and H_2O confirming the partial fragmentation of HCOOH and the subsequent recombination of its fragments into more stable species. The decrease in the intensity of the characteristic bands of formic acid, together with the increase in CO and CO_2 bands, indicates the progressive conversion of the initial compound into oxidized degradation products. Panel b displays the variation in column density of these species as a function of ion fluence.

A systematic decrease in HCOOH and a marked increase in CO_2, CO, and H_2O are observed, particularly at low fluences, followed by a saturation trend at higher fluences. This behavior suggests that chemical conversion is more efficient during the early stages of irradiation when HCOOH is more abundant and that the reaction products tend toward dynamic equilibrium as the ice matrix becomes more processed. Fig. 1b was adapted from the original dataset; according to the authors, the identification of the HCOH species (originally in the figure) was uncertain, and therefore it was excluded from the present figure and the dataset for observed species in this work. However, this species remains in the list of expected species as we will see further.

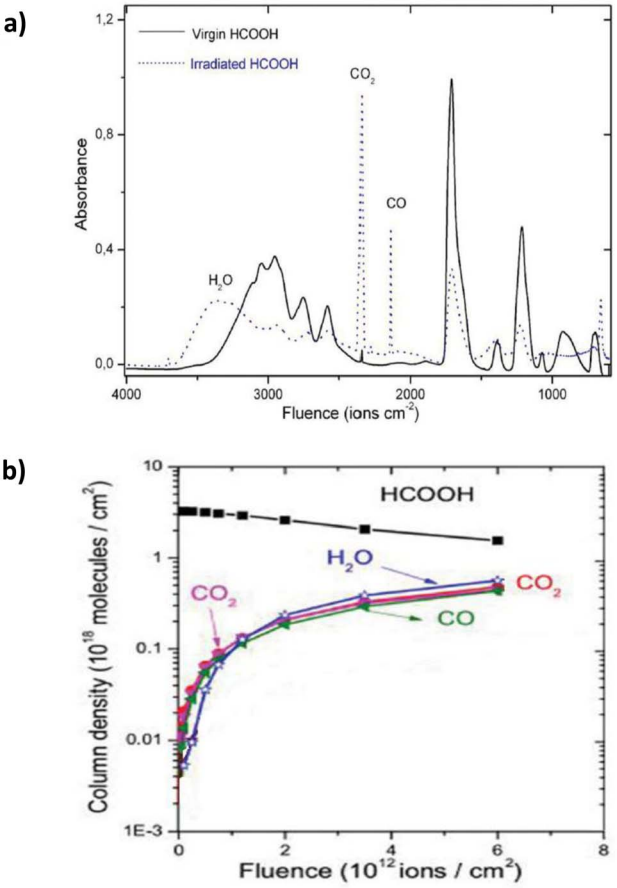

Fig. 1 Infrared spectra and column density evolution of pure HCOOH ice irradiated with 267 MeV Fe ions at 15 K. Panel (a) presents IR spectra of both unirradiated and irradiated ice, highlighting the formation of CO, CO_2, and H_2O bands. Panel (b) illustrates the experimentally measured column density as a function of ion fluence (adapted from Andrade *et al.*[3] (2013)).

2.2 The PROCODA code

In the present work, we employ the python-based PROCODA code (PROgram for Solving Coupled Differential Equations for Astrochemistry) which aims to solve a system of coupled differential equations to describe the chemical evolution of typical astrophysical ices over time when exposed to ionizing radiation processing.[4–6,8,12] Assumptions adopted in the model can be summarized as follows: (1) selected species (which includes the observed species and the expected species) and a selected reaction network including dissociation, bimolecular-collision and desorption channels involving only the selected species; (2) only neutral and radical chemistry is considered, both for computational efficiency and to remain consistent with experimental evidence indicating that neutral and radical pathways dominate the chemistry of cryogenic ices under radiolysis conditions. Although radiolysis can generate ionic species, ionic chemistry is not explicitly included in the present model. This choice is justified by the lack of experimental constraints on ions in FTIR measurements and by the expectation that ions formed in the ice rapidly recombine with secondary electrons, yielding predominantly neutral and radical products. Consequently, neutral and radical pathways are expected to govern the observable ice chemistry; (3) ERCs within reaction groups are thermochemically ranked, favoring exothermic reactions that are more likely to occur at low temperatures (in phase 1 calculations); (4) mass conservation is strictly enforced across all reactions, including desorption processes; (5) the modeled column densities for observed species is forced to be as close as possible than observed values; (6) desorption parameters are tuned to reproduce experimental yields and fluence-dependent behavior; (7) at high ion fluences,

Table 1 Experimental parameters used as input in the PROCODA code in this work (from Andrade *et al.*[3] (2013))

Parameters	Value
Ice initial composition	HCOOH
Radiation flux (Φ)	1.0×10^9 projectile per cm^2 per s
Average projectile energy	267×10^6 eV
Initial column density of ice	3.2×10^{18} molecules per cm^2
Sample thickness	2.0×10^{-4} cm
Sample density	1.22 g cm^{-3}
Sample area	$\sim$0.6 cm^2
Total desorption yield	2.0×10^3 molecules per ion
Sample temperature	15 K

the system is assumed to approach chemical equilibrium,[4] consistent with experimental evidence and ensuring realistic upper limits for molecular concentrations.[4,29]

One of the main advantages of this methodology is its ability to simultaneously quantify the evolution of the column densities of chemical species present in ice. This includes both the species directly observed in the experiments (typically less than 10 species) and a wide range of expected species that may not be immediately detectable. In addition to tracking these chemical transformations, the computational code also calculates the effective rate coefficients (ERCs) for thousands of reactions, providing a comprehensive kinetic analysis. Furthermore, it quantifies the radiation-induced desorption processes, offering insights into how energetic radiation influences the release of molecules from the ice matrix.

The PROCODA computational model operates under a set of structured physicochemical assumptions to simulate the radiolysis-driven chemistry of cryogenic astrophysical ices. These assumptions ensure consistent reaction dynamic, thermodynamic plausibility, and consistency with laboratory constraints.

The current model considers a total of 73 chemical species predicted for pure HCOOH ice were integrated with the four experimentally observed molecules HCOOH, H_2O, CO_2, and CO through a network of 1631 coupled chemical reactions. The full list of the species considered are presented in Appendix A1. The 69 expected species were selected based on several experimental and observational studies that investigated the chemistry of ices containing formic acid (or related compounds), as demonstrated in previous laboratory and astronomical work.[3,20–25] In addition, plausible chemical reactions were considered from the UMIST and KIDA databases.[26,27]

2.2.1 Code workflow. After preparing the experimental dataset to be used in the code, the input file (input information) is included in PROCODA. This file contains the list of chemical species to be modeled, numerical parameters extracted from the experiments, and additional computational variables.

Before running PROCODA, two preliminary modules are executed sequentially: (i) R-GEN PROCODA, which generates the reaction database, and (ii) PRE-PROCODA, which produces the input equations and variable files.

The first of these modules, R-GEN PROCODA, systematically generates the initial set of chemically plausible reactions for the system under study.

Initially, a fixed set of 73 expected molecular species was defined based on observational and experimental astrochemical data representing species whose formation is kinetically and thermodynamically feasible under cryogenic irradiation conditions. This inventory includes molecules already detected experimentally, as well as others considered expected within the modeled environment—species whose synthesis is chemically plausible but remains spectroscopically undetectable. The selected set ensures chemical consistency and astrophysical relevance, forming the basis for the construction of the kinetic reaction network.

Based on this predefined molecular inventory, the R-GEN module automatically generates dissociation (A → B; A → B + C) and bimolecular (A + B → C; A + B → C + D) reaction pathways, initially producing over 20 000 candidate reactions. Since such a large number of reactions is computationally infeasible and many pathways are physically implausible under cryogenic irradiation conditions, a filtering process is applied. This includes: (i) selecting the most exothermic reaction channels, favoring thermodynamically permitted transformations at low temperatures; (ii) the prioritization of reactions involving highly mobile atomic species within the solid matrix, primarily atoms such as H and O.

For this filtering step, specific thresholds are defined for the enthalpy of reaction and for the average diffusion of the reactants within the ice, ensuring that only the most probable reactions are retained. After refinement, the network is reduced to approximately 1600 reactions, a computationally manageable number by PROCODA, forming the final kinetic set implemented in the model. This procedure ensures a chemically consistent and physically grounded process inventory, suitable for simulating the chemistry of radiolysis of formic acid (HCOOH) ice at 15 K.

The final reaction network incorporates only mechanisms with experimental support or thermochemical validation, avoiding speculative or non-physical reactions.[4,12,28] The temporal evolution of each species is modeled using a system of coupled differential equations that describe changes in column density caused by dissociation, bimolecular reactions, and desorption. Reaction rates are expressed as Effective Rate Coefficients (ERCs), parameters specifically adapted from gas-phase kinetics to describe condensed-phase environments.

It is important to note that the PROCODA framework operates with a chemically coherent reaction network, previously validated in different ice systems, allowing the generation of equilibrium projections based on coupled kinetic laws and molecular formation-destruction principles. The calibration of four reference species (HCOOH, H_2O, CO_2, and CO) is used to optimize ERC values, while the broader network remains grounded in bimolecular and radiation-induced processes, supported by thermodynamic data and peer-reviewed scientific literature.

The rate of each effective reaction accounts the availability of the reactants involved up to second order. This is described by the typical system of coupled differential equations used (1) to explain the chemical evolution of astrophysical ices in the PROCODA code.

The equation used to describe the chemical evolution of a given species in the code is given by:

$$\frac{dN_i}{dt} = \left[-\mathrm{DES}_i(t) - \sum_{d_1} k_{d_1} N_i(t) - \sum_{d_2} \frac{k_{d_2} N_i(t) N_a(t)}{L} \right] + \left[\sum_{p_1} k_{p_1} N_a(t) + \sum_{p_2} \frac{k_{p_2} N_a(t) N_b(t)}{L} \right] \left[\text{molecules per cm}^2 \text{ per s}\right] s \quad (1)$$

where N_i as the column density of a given species i, in units of molecules per cm^2, dN_i/dt is the variation in column density over time t, the k values are the ERCs for the different reactions

and L indicates the average sample thickness in units of cm. The term $\mathrm{DES_i}(t) = k_{\mathrm{des,i}}\,\Omega_{\mathrm{i}}(t)N_{\mathrm{i}}(t)$ is the differential estimate of the number of atomic species that are desorbed from the ice into the gas phase per $\mathrm{cm^2}$ and per second due to incident radiation, which also depends on the intrinsic desorption rate ($k_{(\mathrm{des,i})}$), in units of $\mathrm{s^{-1}}$, and the dimensionless surface coverage of species i as a function of time ($\Omega_{\mathrm{i}(t)}$). The equation also has the following parameters: k_{d1} and k_{d2} indicate the processes of destruction (consumption), representing the direct dissociation reactions induced by radiation and have units of $\mathrm{s^{-1}}$, and the values k_{p_1} and k_{p_2} indicate the processes of production of a given species i, representing the bimolecular collision reactions induced by radiation, in units of $\mathrm{cm^{-2}}$ per molecules per s. The N_{a} *e* N_{b} values indicate the column densities of species a and b, respectively, which take part in the reaction to produce or consume the respective species *i*, in units of molecules per $\mathrm{cm^2}$. The full set of employed coupled equations is presented in SI S1.

In the search for the best solution for coupled chemical systems, the score function (SF) was used in the minimization algorithm following eqn (2).

$$\begin{aligned}\mathrm{SF} = {} & p_1 \times \sum \frac{(o\mathrm{HCOOH_{data}} - o\mathrm{HCOOH_{model}})^2}{o\mathrm{HCOOH_{data}}} \\ & + p_2 \times \sum \frac{(o\mathrm{H_2O_{data}} - o\mathrm{H_2O_{model}})^2}{o\mathrm{H_2O_{data}}} + \\ & + p_3 \times \sum \frac{(o\mathrm{CO_{2\ data}} - o\mathrm{CO_{2\ model}})^2}{o\mathrm{CO_{2\ data}}} \\ & + p_4 \times \sum \frac{(o\mathrm{CO_{data}} - o\mathrm{CO_{model}})^2}{o\mathrm{CO_{data}}} \\ & + p_5 \times \left[(1 - \mathrm{MSC_f}) + (1 - \mathrm{MSCo_f}) + (1 - \mathrm{MSCo_m})\right] \\ & + p_6 \times (1 - \mathrm{DSC}) + p_7 \times (1 - \mathrm{SSC}) \qquad (2)\end{aligned}$$

The dimensionless parameters, p_1 to p_7, serve as weights for each term to find the best solution during computational minimization processes. The equation compares the observed column density values of certain species, obtained from the interpolated experimental data, with their respective values calculated by the model. The chi-square function x^2 is a parameter obtained by comparing the experimental column density of observed molecules (HCOOH, H_2O, CO, CO_2) with the modeled column density. It is important to note that the x^2 value can be obtained by setting $p_1 = p_2 = p_3 = p_4 = 1$ and $p_5 = p_6 = p_7 = 0$.

The MSCf parameter (model mass similarity criterion) compares the initial and final column mass of the modeled system, ensuring mass conservation throughout the simulation. It is based on the principle that the sum of atomic masses in reactants must equal that in products an essential foundation of the PROCODA scoring function. MSCof and MSCom represent the similarity between the experimental and modeled column masses at the final and midpoints of the simulation, respectively. Together, these yield the mass similarity criterion $\mathrm{MSC} = (\mathrm{MSC_f} + \mathrm{MSCo_f} + \mathrm{MSCo_m}) \times 100\%/3$, which assesses the model's consistency with observed data. The DSC (desorption similarity criterion) compares the experimental and modeled total desorption yields. The SSC (slope similarity criterion) evaluates whether the model reaches chemical equilibrium, defined by stable concentrations and balanced reaction rates at high radiation fluence, as described in Pilling *et al.*[4] (2022).

2.2.2 Code advantages and limitations. The PROCODA code offers distinct advantages for modeling astrochemical processes in irradiated ices. By integrating thermochemical data in its phase 1 calculations, it refines effective rate coefficients (ERCs) and mitigates degeneracy, yielding realistic predictions of molecular abundances and their evolution during energetic processing. Its ability to resolve formation and destruction pathways, equilibrium abundances, and desorption parameters makes it a bridge between laboratory experiments and astrochemical models, with applications from dense molecular clouds and protoplanetary disks to icy solar system bodies.

PROCODA currently includes only neutral and radical species, since ionic products rapidly neutralize *via* recombination with secondary electrons.[30,31] The model operates on a predefined reaction network that simplifies amorphous-ice microphysics and treats irradiation through fluence rather than explicit projectile energy or mass parameters known to influence chemical pathways and equilibrium states,[7,9,32,33,38] which will be incorporated in future implementations.

It is important to note that, under cryogenic conditions, not only isolated radicals but also weakly bound radical–molecule complexes may play a relevant role in the early stages of radiation-induced chemistry. Experimental matrix-isolation studies have shown that complexes such as OH···CO or HO···CO can be efficiently formed under UV or X-ray irradiation and may act as precursors to more stable species, including the HOCO radical. In highly rigid ice matrices, where molecular diffusion and reorientation are severely restricted, such complexes can effectively trap reactive partners and influence reaction outcomes. While these species are not treated explicitly as distinct chemical entities in the present macrokinetic framework, their chemical effects are implicitly accounted for through effective reaction pathways and rate coefficients.

Considering the model's core assumptions—(i) the tendency toward chemical equilibrium at high fluences; (ii) thermochemical selection favoring exothermic reactions (during phase 1 calculations); (iii) strict mass conservation; (iv) consistency with experimental desorption data; and (v) quadratic χ^2 minimization guided by spectroscopic datasets—the degeneracy of numerical solutions is significantly reduced, favoring convergence toward the global minimum. As a result, the average uncertainty associated with simulated molecular abundances remains around ~20%,[4–6] in line with previous studies (see Pilling *et al.*[4] 2022).

3. Results and discussion

This section presents the main results obtained, highlighting the molecular abundances at chemical equilibrium. Subsection

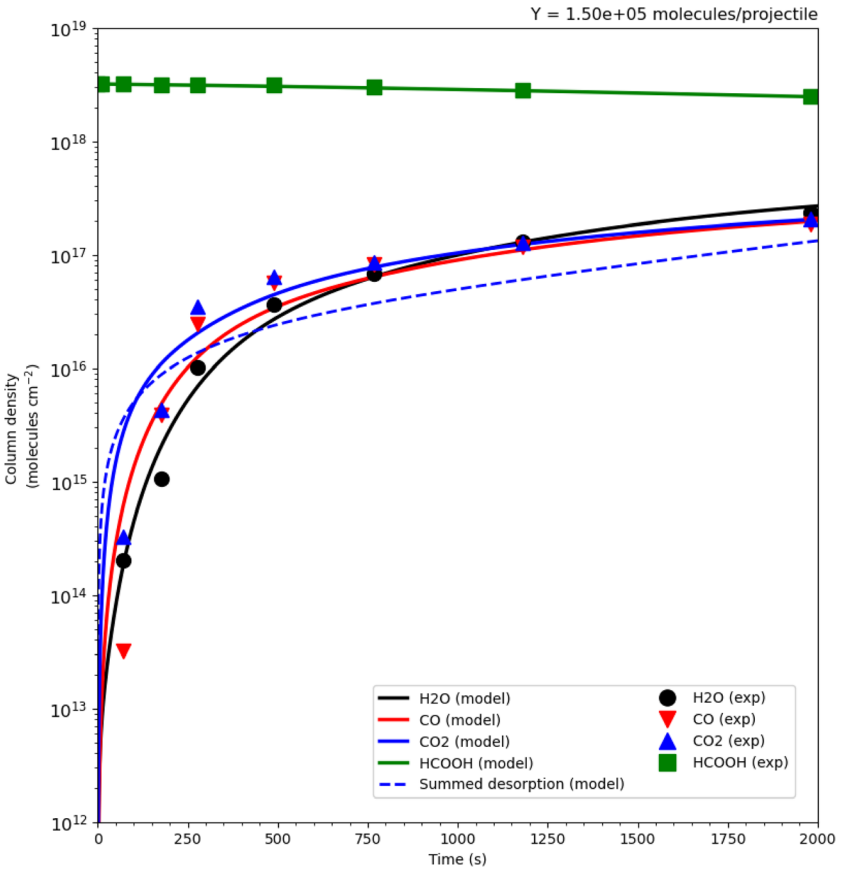

Fig. 2 Best-fit models showing the evolution the column densities of the 4 observed species in the experiment (H_2O, CO, CO_2 and HCOOH). The modeled summed desorption is presented by blue dashed line. The calculated desorbed yield was $Y = 1.5$ molecules per projectile. Experimental data points from Andrade *et al.*[3] (2013). See details in the text.

3.1 discusses the best-fitting model, including the temporal evolution of the abundances of the 73 simulated species under irradiation, also examining the relative abundances achieved at chemical equilibrium. Subsection 3.2 addresses radiation-induced desorption in pure HCOOH ice at 15 K, as well as the species that exhibit significant desorption in the simulation. Subsection 3.3 analyzes the most relevant reactions in the formation and destruction of simulated species such as HCOOH, H_2O, CO, CO_2, H, OH, H_2CO, CH_2OH, CH_3O, HCO, H_2O_2, and HOCO in irradiated molecular ices, based on the effective rate coefficients (ERCs) calculated by the PROCODA code. These simulated and experimentally detected species are particularly relevant from a physicochemical and astrochemical perspective. Subsection 3.4 provides a comparison with other models already simulated by PROCODA, based on the results obtained.

3.1 The best-fit model

Fig. 1 presents the modeled column densities (in molecules cm^2) for the species observed in pure HCOOH ice irradiated at 15 K by 267 MeV $^{56}Fe^{22+}$ ions. The experimental data from Andrade *et al.*[3] (2013) are also indicated in the figure by discrete symbols and serve as a reference for model validation. The chemical equilibrium phase, which, according to the PROCODA simulation, is reached in approximately 2000s (horizontal plateau at long exposure times). Although the full simulation spans 6000s, the selected snapshot emphasizes the equilibrium condition, where the rate of formation and destruction of chemical species becomes stationary. The model shows very good agreement with the experimental data. The total desorption yield (Y) predicted by the model was 1.50×10^5 molecules per projectile approximately an order of magnitude higher than the value estimated by the authors from experimental measurements. This improvement can be attributed to the methodology's ability to monitor species that were not mapped during the experiments (Fig. 2).

The modeled column densities for the 73 chemical species simulated in PROCODA are presented in the Fig. 3, distributed in panels a to f in decreasing order of abundance, which reflects an organization strategy that allows visually identifying the most relevant species in the chemical evolution induced by ionizing radiation in astrophysical ices. Panels a, b, and c display the species with the highest column densities, exceeding 10^{14} mol cm^{-2}, indicating that these molecules, such as CO_2, CO, H_2O, HCOOH, H_2, CH_4, CH_2OH, CH_3OH, and OH, play central roles in the modeled system, either due to their high chemical stability or their efficient formation from major radiolytic pathways. Panels d, e, and f show less abundant

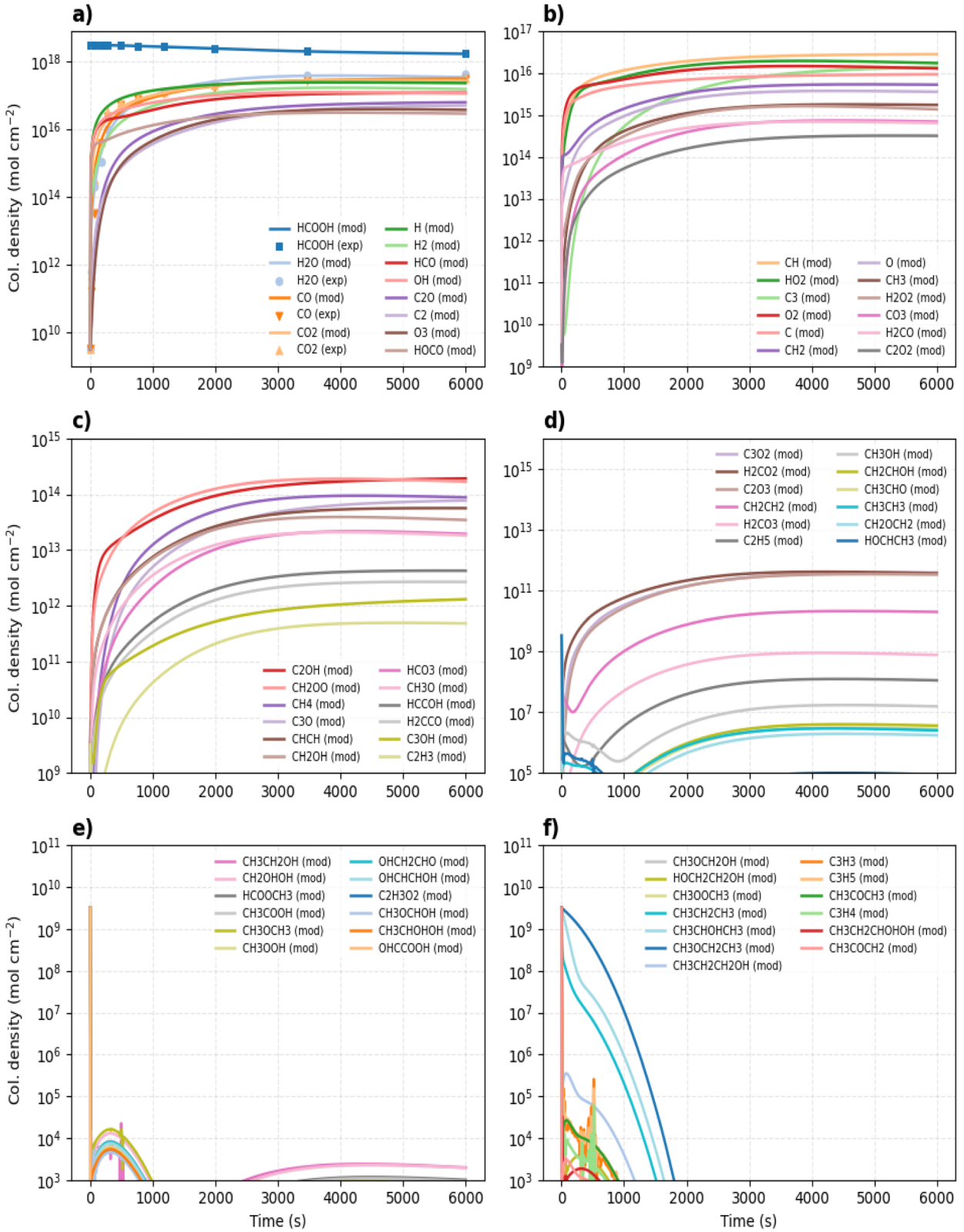

Fig. 3 Best-fit models showing the evolution of column densities of the 73 species observed in the experiment (organized by abundance in the chemical equilibrium phase). Experimental data points from Andrade *et al.*[3] (2013). Panels (a–c) indicate the most important species, while panels (d–f) indicate the least important species. See details in the text.

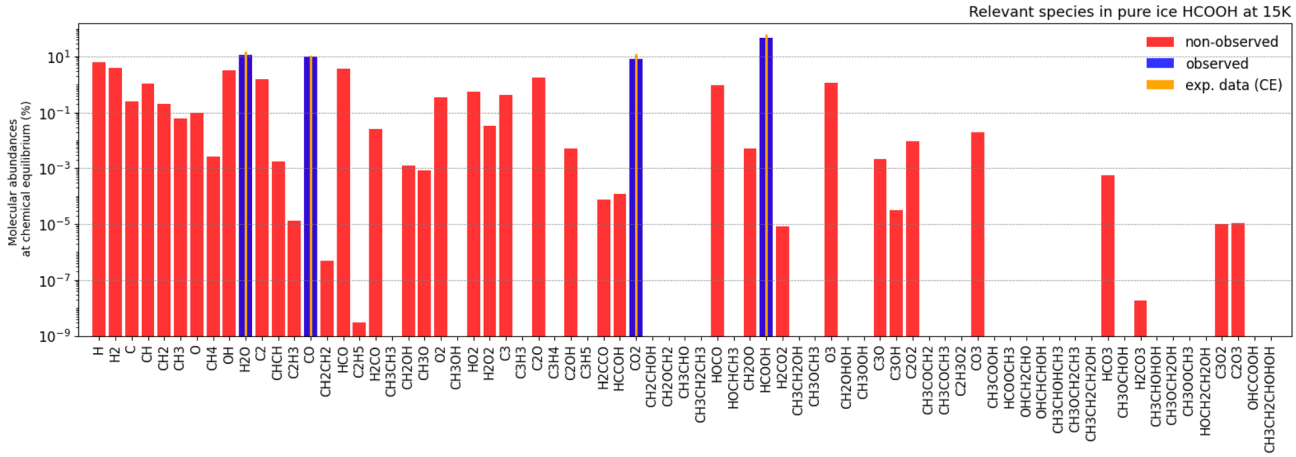

Fig. 4 Modeled molecular abundances (>10^{-9} %) at chemical equilibrium for irradiated HCOOH ice (15 K). Blue bars show species reproduced by the model and experimentally detected; red bars represent predicted but unobserved products; orange thin lines mark experimental values for comparison.

species, generally below 10^9 mol cm^{-2}, many of which are reactive intermediates or low-probability products formed in secondary reaction steps, such as CH_3, CH_2, CH_3CH_2OH, CH_3-CH_2OCH_3, CH_3COOH and $OHCH_2CH_2OH$, whose transient presence reflects their highly reactive nature and their participation in reaction chains that lead to the formation of more stable compounds.

This hierarchical organization, evident in the subgraphs, allows PROCODA to efficiently quantify and classify the species according to their chemical relevance, adopting as a minimum significance criterion a value of 10^9 mol cm^{-2} on the logarithmic scale, which highlights a robust approach for analyzing molecular complexification in simulated astrophysical environments.

It is noteworthy that the simulated trends for key species such as CO, CO_2, H_2O, and HCOOH agree with experimental data, corroborating the model's expected ability. These results demonstrate the efficiency of the PROCODA code in reproducing radiation-induced molecular synthesis under conditions typical of astrophysical ices. The ability to simulate, within an integrated kinetic framework, both transient and stable species is fundamental to understanding the chemical evolution of ice in environments such as dense molecular clouds, protoplanetary disks, and icy bodies in the Solar System.

The correspondence between simulation and experiment is particularly satisfactory for the most abundant molecules, confirming the kinetic network implemented in PROCODA. Light species, such as H_2, CO, CO_2, OH, HCO, and H_2CO, exhibit the highest column densities due to their rapid formation from the primary dissociation of HCOOH. Because they have low molecular weight, simple structure, and high mobility in ice, these molecules are favored both in the initial formation stage and in their stabilization over time. Furthermore, because they are direct products of molecular fragmentation or intermediates of highly exothermic reactions, these species are produced in large quantities already in the early stages of the simulation and remain in high concentrations throughout the irradiation period. In simulations of pure HCOOH ice, PROCODA predicts partial recombination of HCOOH itself from radiolysis-generated fragments, such as CO and OH, *via* reaction pathways such as CO + OH → HCOOH. This behavior reflects a dynamic balance between fragmentation and recombination, widely observed in experiments with ice irradiated with heavy ions. The apparent increase in HCOOH abundance over time should be interpreted as a result of chemical recycling, not primary synthesis, reinforcing its role as the dominant parent species in radiation-induced chemistry.

A central focus of this work was the differentiation between species considered relevant and irrelevant among the initial chemical components used to fit the experimental data of pure HCOOH ice subjected to irradiation. The species classified as relevant, that is, those that contributed most to the final chemical composition (*e.g.*, H, H_2, C, CH, CH_2, CH_3, O, CH_4, OH, H_2O, C_2, CHCH, C_2H_3, CO, CH_2CH_2, HCO, H_2CO, CH_2OH, CH_3O, O_2, HO_2, H_2O_2, C_3, C_2O, C_2OH, H_2CCO, HCCOH, CO_2, HOCO, CH_2OO, HCOOH, H_2CO_2, O_3, C_3O, C_3OH, C_2O_2, CO_3, HCO_3, C_3O_2, and C_2O_3). Altogether, these species represent approximately 55% of all chemistry investigated in this study. The quantitative values of the evolution of column densities and desorption processes—normalized in relation to the parental species are detailed in SI S3, based on the best-fit model applied.

Fig. 4 shows the molecular abundances at chemical equilibrium (logarithmic scale, in %) of the 42 relevant species (>10^{-9} %) in the best-fit model for pure HCOOH ice irradiated at 15 K. The values correspond to the final stage of the simulation with the PROCODA code, when production and destruction rates are balanced. Blue bars indicate species experimentally detected by Andrade *et al.*[3] (2013), while red bars represent products predicted only by the model. Orange lines above the blue bars show the abundances measured in the laboratory, allowing direct comparison with the simulated results. The overlay confirms good agreement between experimental data and modeling, demonstrating the robustness of PROCODA. The

Table 2 Numerical values for the modeled abundances at the chemical equilibrium phase in the pure HCOOH ice 15 K ice modeled by PROCODA

Species	Abundances at chemical equilibrium (molecules per cm^2)	Abundances at chemical equilibrium (%)
H	2.4×10^{17}	6.6×10^{0}
H_2	1.6×10^{17}	4.4×10^{0}
C	9.6×10^{15}	2.6×10^{-1}
CH	2.9×10^{16}	7.9×10^{-1}
CH_2	5.4×10^{15}	1.5×10^{-1}
CH_3	1.8×10^{15}	4.9×10^{-2}
O	3.7×10^{15}	1.1×10^{-1}
CH_4	8.8×10^{13}	2.5×10^{-3}
OH	1.2×10^{17}	3.3×10^{0}
H_2O	3.6×10^{17}	9.9×10^{0}
C_2	5.3×10^{16}	1.5×10^{0}
CHCH	5.7×10^{13}	1.6×10^{-3}
C_2H_3	4.9×10^{11}	1.4×10^{-5}
CO	3.3×10^{17}	8.9×10^{0}
CH_2CH_2	1.9×10^{10}	5.4×10^{-7}
HCO	1.3×10^{17}	3.4×10^{0}
C_2H_5	1.2×10^{8}	3.0×10^{-9}
H_2CO	6.5×10^{14}	1.8×10^{-2}
CH_2OH	3.5×10^{13}	9.6×10^{-4}
CH_3O	1.9×10^{13}	5.0×10^{-4}
O_2	1.3×10^{16}	3.5×10^{-1}
HO_2	1.8×10^{16}	4.9×10^{-1}
H_2O_2	1.4×10^{15}	3.9×10^{-2}
C_3	1.4×10^{16}	3.4×10^{-1}
C_2O	6.5×10^{16}	1.8×10^{0}
C_2OH	1.9×10^{14}	5.3×10^{-3}
H_2CCO	2.7×10^{12}	7.4×10^{-5}
HCCO	4.3×10^{12}	1.2×10^{-4}
CO_2	2.9×10^{17}	7.8×10^{0}
HOCO	2.9×10^{16}	8.3×10^{-1}
CH_2OO	1.7×10^{14}	4.7×10^{-3}
HCOOH	1.8×10^{18}	4.8×10^{1}
H_2CO_2	3.7×10^{11}	1.0×10^{-5}
O_3	3.9×10^{16}	1.0×10^{0}
C_3O	7.8×10^{13}	2.1×10^{-3}
C_3OH	1.3×10^{12}	3.6×10^{-5}
C_2O_2	3.3×10^{14}	8.9×10^{-3}
CO_3	7.0×10^{14}	1.9×10^{-2}
HCO_3	1.9×10^{13}	5.4×10^{-4}
H_2CO_3	7.7×10^{8}	2.0×10^{-8}
C_3O_2	3.8×10^{11}	1.0×10^{-5}
C_2O_3	3.3×10^{11}	9.1×10^{-6}

inclusion of undetected species broadens the understanding of the radiation-induced chemical network, highlighting the complexity of chemical evolution in ices. These results reinforce the importance of considering predicted intermediates, especially under low-temperature and high-radiation conditions typical of dense clouds or icy surfaces.

Table 2 presents the numerical values of molecular abundances in the chemical equilibrium phase for pure HCOOH ice at 15 K, obtained from the best-fit simulation using the PROCODA code. These values represent the steady-state concentrations after prolonged exposure to ionizing radiation, where the rates of molecular formation and destruction are balanced. The results reflect both experimentally observed molecules and predicted species, providing a comprehensive view of the chemical inventory within the processed ice. The application of physical chemistry in this context is fundamental: it allows for the precise quantification of the elementary processes of dissociation, recombination, and the cause of radiation on the ice, integrating thermodynamic and kinetic aspects into the modeling. The PROCODA code provides robust estimates of equilibrium abundances for the chemical parameters involved by solving coupled differential equations grounded in experimental data and physico-chemical principles.

3.2 Radiation-induced molecular desorption

Fig. 5 shows the percentage distribution of molecular species desorbed by irradiation under chemical equilibrium conditions, as simulated for pure HCOOH ice with the PROCODA code. This result corresponds to the point in the simulation at which molecular formation and destruction reach a steady state, characterizing the chemical equilibrium phase of the system. Only species with desorption yields greater than 10^{-5} % were included to highlight the main contributors to the gas phase composition. The blue bars represent experimentally detected molecules, while the red bars correspond to species predicted exclusively by the model. The analysis highlights which molecules are most efficiently released from the ice matrix under the effect of ionizing radiation. In this context, it is essential to emphasize that the desorption considered in this simulation is caused by sputtering a process driven by heavy cosmic rays, such as $^{56}Fe^{22+}$ ions, which deposit enough energy to eject molecules directly from the ice at low temperatures also spoken by Dartois *et al.*[33] (2015). This mechanism is highly relevant in cold astrophysical environments, where the temperature does not allow significant thermal sublimation, making sputtering the primary pathway for volatile release into the gaseous medium.

As indicated in the Fig. 5, light and highly mobile species, such as H, H_2, OH, and O, dominate equilibrium desorption, reflecting their greater efficiency in escaping the matrix after collision with energetic particles. The H_2O molecule also exhibits significant desorption, consistent with its high initial concentration and its role as the main structural constituent of ice. The presence of HCOOH, H_2O, and CO in the gas phase reinforces the combined action of irradiation-induced fragmentation processes and recombination of reactive intermediates. These results align with the chemical mechanisms embedded in PROCODA, especially in the best-fit models. In summary, the simulated data validates the predictive capacity of PROCODA to describe, with astrophysical relevance, the main sputtering desorption pathways in ices processed by cosmic rays.

It is important to note that the PROCODA model does not make individual adjustments for each species based on their desorption rates. Instead, the code simulates the overall chemical dynamics of the system, calibrating the reaction parameters to ensure that the total sum of desorbed species is compatible with the integrated experimental desorption yields. This approach allows for greater robustness in modeling astrochemical environments where multiple reaction pathways

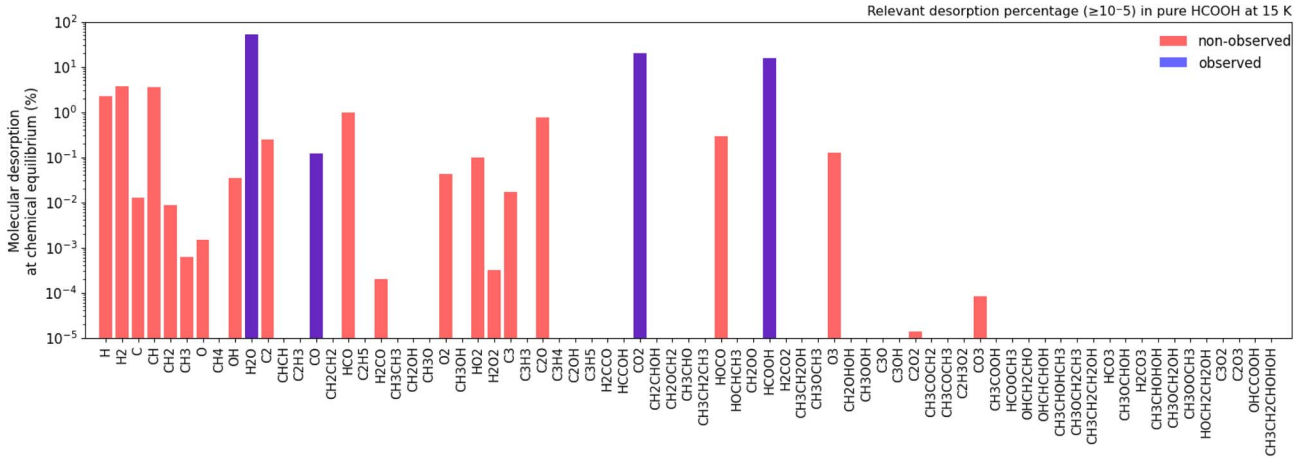

Fig. 5 Simulated radiation-induced desorption yields (>10^{-5} %) for pure HCOOH ice at 15 K under Fe-ion irradiation. Blue bars correspond to experimentally observed species; red bars indicate additional species predicted by PROCODA.

and competing processes occur simultaneously. Additionally, in the case of pure HCOOH ice irradiated with $^{56}Fe^{22+}$ projectile, the PROCODA model estimates a total desorption yield of 1.5×10^5 molecules per projectile, compared to the experimental value of 2.0×10^3 molecules per projectile reported by Andrade *et al.*[3] (2013). This discrepancy nearly two orders of magnitude is not indicative of a modeling error but reflects an intrinsic feature of PROCODA. The code is designed to reproduce the global system dynamics and the integrated desorption fluxes rather than fit individual species. Its strength lies in capturing the total desorbed molecular production, including light species such as H, OH, and H_2, which can escape experimental detection due to instrumental limitations. This holistic approach allows PROCODA to represent collective desorption behavior more comprehensively than experiments alone.

Based on the PROCODA simulation, it is observed that, at the beginning of the simulation, before chemical equilibrium is reached, desorption is dominated by HCOOH, due to its high initial concentration in pure ice and its ease of ejection by sputtering. Thus, formic acid is efficiently removed from the matrix in the first energy deposition events. As the system evolves under continuous irradiation, there is an increase in the production of secondary species, especially H_2O, generated by the fragmentation of HCOOH and the recombination of

Table 3 Numerical values for the modeled desorption in the chemical equilibrium phase on ice of pure HCOOH at 15 K modeled by PROCODA

Species	Desorption in column densities at chemical equilibrium (molecules per cm^2)	Desorption in percentage at chemical equilibrium (%)
H	1.4×10^{16}	2.8×10^{0}
H_2	2.7×10^{16}	5.4×10^{0}
C	7.2×10^{16}	1.4×10^{-2}
CH	1.1×10^{16}	2.2×10^{0}
CH_2	2.2×10^{13}	4.5×10^{-3}
CH_3	1.9×10^{12}	3.7×10^{-4}
O	8.2×10^{12}	1.6×10^{-3}
OH	2.2×10^{14}	4.5×10^{-2}
H_2O	2.4×10^{17}	4.9×10^{1}
C_2	1.0×10^{15}	2.1×10^{-1}
CO	1.3×10^{15}	2.6×10^{-1}
HCO	6.2×10^{15}	1.2×10^{0}
H_2CO	3.7×10^{11}	7.6×10^{-5}
O_2	2.2×10^{14}	4.5×10^{-2}
HO_2	3.8×10^{14}	7.8×10^{-2}
H_2O_2	2.1×10^{12}	4.4×10^{-4}
C_3	6.2×10^{13}	1.2×10^{-2}
C_2O	3.5×10^{15}	7.1×10^{-1}
CO_2	1.0×10^{17}	2.1×10^{1}
HOCO	1.0×10^{15}	1.6×10^{-1}
HCOOH	7.8×10^{16}	1.5×10^{1}
O_3	5.5×10^{14}	1.1×10^{-1}
C_2O_2	8.7×10^{10}	1.7×10^{-5}
CO_3	4.5×10^{11}	9.1×10^{-5}

intermediates such as H_2O and OH. At chemical equilibrium, H_2O begins to dominate desorption, surpassing HCOOH in percentage yield in the gas phase.

Table 3 presents the numerical values for modeled desorption in pure HCOOH ice at 15 K, as simulated using the PROCODA code. The values correspond to the chemical equilibrium stage, where the formation and destruction rates are balanced. For each species, we report the equilibrium column density of desorbed molecules (molecules per cm^2), the fractional desorption yields relative to the total equilibrium abundance (%), and the average desorption rate (s^{-1}). These values quantify the steady-state release of molecules into the gas phase under prolonged irradiation and provide constraints for the interpretation of observational data in cold, dense interstellar environments.

A key focus of this research is the role of radiation-induced desorption in facilitating the transition of chemical species such as formic acid (HCOOH) from the ice phase to the gas phase. This mechanism enables molecules formed within icy mantles to become detectable by high-sensitivity radio telescopes, such as ALMA, in protoplanetary disks and other young astrophysical environments (*e.g.*, Öberg *et al.*,[34] 2021). The findings contribute to a deeper understanding of how volatile compounds are retained and subsequently released, offering predictive insights for astronomical detection efforts in the millimeter and submillimeter wavelength ranges. Although HCOOH is not commonly observed in protoplanetary disks, its detection in star-forming regions such as the L1157-B1 protostellar shock Lefloch *et al.*,[35] (2017) underscores the significance of desorption processes in delivering these molecules to the gas phase.

3.3 Dominant reaction pathways for selected species

In this section, we analyze the main reaction pathways that govern the system's kinetics, identifying for each species the two most important formation routes and the two most significant consumption routes. Table 4 presents these dominant pathways for the selected species (HCOOH, H_2O, CO, CO_2, H, OH, HCO, H_2CO, CH_2OH, CH_3O, H_2O_2 and HOCO), detailing key reactions within the model. This approach emphasizes the kinetic mechanisms of greatest relevance, highlighting how atom-abstraction and radical–recombination reactions drive chemical dynamics. By focusing on dominant pathways, we simplify the physicochemical interpretation of the results: for example, we can identify which intermediate radicals are generated and which routes lead to the production or consumption of each molecule under irradiation. This table thereby indicates which reactions account for the largest fraction of chemical conversion, clarifying common trends and enabling correlations with known low-temperature reactivity mechanisms.

In general terms, the dominant formation reactions typically involve hydrogen addition to oxygenated radicals. For instance, the recombination of the HOCO radical with atomic hydrogen (H + HOCO → HCOOH) appears as the main route for HCOOH formation, illustrating a hydrogenation process of a hydrocarbonyl radical. Similarly, hydrogenation pathways regenerate water and other compounds: for example, OH + H_2 → H_2O produces water from OH radicals, and H + HCO → H_2 + CO forms CO *via* hydrogen abstraction from HCO. This pattern reflects a cycle of radical reactions in which atomic hydrogen reconstitutes stable molecules.

Accordingly, Andrade *et al.*[3] (2013) identified that the most abundant products from the irradiation of solid HCOOH are precisely CO, CO_2, and H_2O, consistent with the hydration and oxidation routes observed. The participation of the CH_2OO radical, present as a reactant in formation channels (*e.g.*, H + CH_2OO → HCOOH), suggests the formation of oxygenated organic intermediates within the reaction network, although the exact role of this complex radical is not yet fully clarified.

The dominant destruction reactions, in turn, are characterized by hydrogen abstraction and partial oxidation of the species. For example, the oxygen atom acts as an abstractor in the pathway O + HCOOH → OH + HOCO, which removes hydrogen from HCOOH to produce the radicals HOCO and OH. The HOCO radical thus generated acts as a critical intermediate, since its subsequent hydrogenation (H + HOCO → H_2 + CO_2) leads to CO_2 formation, completing the oxidation of HCOOH. This behavior has been highlighted in radiolysis studies, where HOCO is identified as a key primary product.[36] Ryazantsev and Feldman[36](2015) experimentally confirmed that HOCO is a major product of the radiolytic decomposition of HCOOH, acting as a primary dissociation pathway. This pattern is reflected in our model: multiple pathways involve HOCO, both in its generation (from HCOOH destruction) and in its consumption (to form CO_2).

Other abstraction-driven channels are also recurrent, such as C + HCO → CH + CO and H + HCO → H_2 + CO, efficiently converting the HCO radical into CO and favoring its accumulation. This result is consistent with the findings of Pilling *et al.*[2] (2006), who reported that the CO^+ fragment dominates the dissociation spectra of gaseous HCOOH under energetic impact, indicating that CO formation is a characteristic feature of formic acid decomposition.

Beyond radiolysis-driven degradation pathways, complementary experimental studies have demonstrated that radiation-induced chemistry in cryogenic ice complexes can also proceed in the reverse direction, leading to the formation of HCOOH. In particular, irradiation of weakly bound $H_2O\cdots CO$ and $H_2O\cdots CO_2$ complexes has been shown to efficiently produce the HOCO radical, either directly or *via* transient radical–molecule complexes such as OH···CO, which subsequently evolve into formic acid upon hydrogen addition. These results indicate that both degradation and synthetic pathways involving HOCO intermediates may coexist in astrophysical ices under irradiation, with the dominant route depending on the initial ice composition and local physicochemical environment.

In summary, the dominant reaction channels exhibit a coherent pattern: the destruction of complex molecules occurs mainly through hydrogen abstraction (producing radicals such as HOCO, OH, and HCO), whereas the formation of stable molecules occurs *via* hydrogenation of these radicals. HOCO and OH appear as key intermediates in several species,

Table 4 Dominant two-most formation and consumption reaction pathways for selected species (HCOOH, H_2O, CO, CO_2, H, OH, HCO, H_2CO, CH_2OH, CH_3O, H_2O_2 and HOCO) computed with the PROCODA code for the studied irradiated HCOOH ice (*r* in the table corresponds to the reaction)[a]

	Low-dose irradiated ice (beginning of experiment) [reaction label; effective reaction rate]	Highly irradiated ice (CE phase) [reaction label and effective reaction rate]
HCOOH		
Formation pathway		
1st reaction	H + HOCO → HCOOH [r_{235}; 4.9×10^{-23} molecules per cm^3 per s]	H + HOCO → HCOOH [r_{235}; 4.9×10^{-23} molecules per cm^3 per s]
2nd reaction	H + CH_2OO → H + HCOOH [r_{780}; 4.3×10^{-23} molecules per cm^3 per s]	H + CH_2OO → H + HCOOH [r_{780}; 4.3×10^{-23} molecules per cm^3 per s]
Consumption pathway		
1st reaction	O + HCOOH → OH + HOCO [r_{1240}; 3.2×10^{-23} molecules per cm^3 per s]	O + HCOOH → OH + HOCO [r_{1240}; 3.2×10^{-23} molecules per cm^3 per s]
2nd reaction	HCOOH + R → OH + HCO [r_{571}; 3.3×10^{-5} molecules per cm^3 per s]	HCOOH + R → OH + HCO [r_{571}; 3.3×10^{-5} molecules per cm^3 per s]
H_2O		
Formation pathway		
1st reaction	H_2 + OH → H + H_2O [r_{119}; 2.9×10^{-23} molecules per cm^3 per s]	H_2 + OH → H + H_2O [r_{119}; 2.9×10^{-23} molecules per cm^3 per s]
2nd reaction	H_2O_2 + R → O + H_2O [r_{112}; 5.7×10^{-1} molecules per cm^3 per s]	H_2O_2 + R → O + H_2O [r_{112}; 5.7×10^{-1} molecules per cm^3 per s]
Consumption pathway		
1st reaction	H + H_2O → H_2 + OH [r_{118}; 7.9×10^{-24} molecules per cm^3 per s]	H + H_2O → H_2 + OH [r_{118}; 7.9×10^{-24} molecules per cm^3 per s]
2nd reaction	H_2O + R → H + OH [r_{100}; 2.9×10^{-3} molecules per cm^3 per s]	H_2O + R → H + OH [r_{100}; 2.9×10^{-3} molecules per cm^3 per s]
CO		
Formation pathway		
1st reaction	H + HCO → H_2 + CO [r_{718}; 1.4×10^{-23} molecules per cm^3 per s]	H + HCO → H_2 + CO [r_{718}; 1.4×10^{-23} molecules per cm^3 per s]
2nd reaction	C_2O + R → C + CO [r_{143}; 1.0×10^{-2} molecules per cm^3 per s]	C_2O + R → C + CO [r_{753}; 1.0×10^{-2} molecules per cm^3 per s]
Consumption pathway		
1st reaction	H + CO → HCO [r_{219}; 5.9×10^{-24} molecules per cm^3 per s]	H + CO → HCO [r_{219}; 5.9×10^{-24} molecules per cm^3 per s]
2nd reaction	CO + O_2 → CO_3 [r_{177}; 4.6×10^{-23} molecules per cm^3 per s]	CO + O_2 → CO_3 [r_{177}; 4.6×10^{-23} molecules per cm^3 per s]
CO_2		
Formation pathway		
1st reaction	H + HOCO → H_2 + CO_2 [r_{463}; 3.2×10^{-23} molecules per cm^3 per s]	H + HOCO → H_2 + CO_2 [r_{463}; 3.2×10^{-23} molecules per cm^3 per s]
2nd reaction	HOCO + R → H + CO_2 [r_{230}; 1.7×10^{-2} molecules per cm^3 per s]	HOCO + R → H + CO_2 [r_{230}; 1.7×10^{-2} molecules per cm^3 per s]
Consumption pathway		
1st reaction	H + CO_2 → HOCO [r_{231}; 6.9×10^{-24} molecules per cm^3 per s]	H + CO_2 → HOCO [r_{231}; 6.9×10^{-24} molecules per cm^3 per s]
2nd reaction	C + CO_2 → CO + CO [r_{188}; 1.7×10^{-23} molecules per cm^3 per s]	C + CO_2 → CO + CO [r_{188}; 1.7×10^{-23} molecules per cm^3 per s]
H		
Formation pathway		
1st reaction	H + H → H_2 [r_2; 5.0×10^{-23} molecules per cm^3 per s]	H + CO_2 → HOCO [r_{231}; 6.9×10^{-24} molecules per cm^3 per s]
2nd reaction	HCOOH + R → H + HOCO [r_{234}; 2.5×10^{2} molecules per cm^3 per s]	C + H_2O_2 → H + HOCO [r_{764}; 3.10×10^{24} molecules per cm^3 per s]
Consumption pathway		
1st reaction	H + H → H_2 [r_2; 5.0×10^{-23} molecules per cm^3 per s]	H + H → H_2 [r_2; 5.0×10^{-23} molecules per cm^3 per s]
2nd reaction	H + HOCO → H_2 + CO_2 [r_{763}; 3.2×10^{-23} molecules per cm^3 per s]	H + H_2O → H_2 + OH [r_{118}; 7.9×10^{-2} molecules per cm^3 per s]
OH		
Formation pathway		
1st reaction	O + HCOOH → OH + HOCO [r_{1240}; 3.2×10^{-23} molecules per cm^3 per s]	H + H_2O → H_2 + OH [r_{118}; 7.79×10^{-24} molecules per cm^3 per s]
2nd reaction	H_2O_2 + R → OH + OH [r_{114}; 1.8×10^{-1} molecules per cm^3 per s]	H_2O + R → H + OH [r_{100}; 2,6 $\times 10^{-3}$ molecules per cm^3 per s]

Table 4 (*Contd.*)

	Low-dose irradiated ice (beginning of experiment) [reaction label; effective reaction rate]	Highly irradiated ice (CE phase) [reaction label and effective reaction rate]
Consumption pathway		
1st reaction	$OH + OH \rightarrow H_2 + O_2$ [r_{134}; 8.8×10^{-24} molecules per cm^3 per s]	$H_2 + OH \rightarrow H + H_2O$ [r_{119}; 2.9×10^{-23} molecules per cm^3 per s]
2nd reaction	$OH + OH \rightarrow H + HO_2$ [r_{125}; 6.8×10^{-24} molecules per cm^3 per s]	$OH + OH \rightarrow H_2 + O_2$ [r_{134}; 8.8×10^{-24} molecules per cm^3 per s]
HCO		
Formation pathway		
1st reaction	$HCOOH + R \rightarrow OH + HCO$ [r_{571}; 3.3×10^{-5} molecules per cm^3 per s]	$H + CO \rightarrow HCO$ [r_{219}; 5.9×10^{-24} molecules per cm^3 per s]
2nd reaction	$C + HOCO \rightarrow CO + HCO$ [r_{1076}; 2.9×10^{-23} molecules per cm^3 per s]	$CH_2OO + R \rightarrow OH + HCO$ [r_{570}; 3,4 $\times 10^{-1}$ molecules per cm^3 per s]
Consumption pathway		
1st reaction	$HCO + R \rightarrow H + CO$ [r_{218}; 1.2×10^{-3} molecules per cm^3 per s]	$H + HCO \rightarrow H2 + CO$ [r_{718}; 1.4×10^{-23} molecules per cm^3 per s]
2nd reaction	$H + HCO \rightarrow H_2 + CO$ [r_{718}; 1.4×10^{-23} molecules per cm^3 per s	$C + HCO \rightarrow CH + CO$ [r_{1054}; 2.9×10^{-23} molecules per cm^3 per s]
H_2CO		
Formation pathway		
1st reaction	$HCOOH + R \rightarrow O + H_2CO$ [r_{461}; 8.0×10^{-7} molecules per cm^3 per s]	$CH_2OO + R \rightarrow O + H_2CO$ [r_{459}; 2.1×10^{-1} molecules per cm^3 per s]
2nd reaction	$CH_2OO + R \rightarrow O + H_2CO$ [r_{459}; 2.1×10^{-1} molecules per cm^3 per s]	$H + HCO \rightarrow H_2CO$ [r_{221}; 1.3×10^{-25} molecules per cm^3 per s]
Consumption pathway		
1st reaction	$H_2CO + R \rightarrow H + HCO$ [r_{220}; 2.3×10^{-2} molecules per cm^3 per s]	$H + H_2CO \rightarrow CH_2OH$ [r_{223}; 5.03×10^{-23} molecules per cm^3 per s]
2nd reaction	$H_2CO + R \rightarrow H_2 + CO$ [r_{264}; 2.0×10^{-2} molecules per cm^3 per s]	$H + H_2CO \rightarrow CH_3O$ [r_{225}; 2.4×10^{-23} molecules per cm^3 per s]
CH_2OH		
Formation pathway		
1st reaction	$H + H_2CO \rightarrow CH_2OH$ [r_{223}; 5.03×10^{-23} molecules per cm^3 per s]	$H + H_2CO \rightarrow CH_2OH$ [r_{223}; 5.03×10^{-23} molecules per cm^3 per s]
2nd reaction	$H + CH_2OO \rightarrow O + CH_2OH$ [r_{786}; 1.5×10^{-23} molecules per cm^3 per s]	$H + CH_2OO \rightarrow O + CH_2OH$ [r_{786}; 1.5×10^{-23} molecules per cm^3 per s]
Consumption pathway		
1st reaction	$CH_2OH + R \rightarrow H_2 + H_2CO$ [r_{265}; 4.8×10^{-1} molecules per cm^3 per s]	$CH_2OH + R \rightarrow H_2 + H_2CO$ [r_{265}; 4.8×10^{-1} molecules per cm^3 per s]
2nd reaction	$CH_2OH + R \rightarrow H + H_2CO$ [r_{222}; 4.6×10^{-1} molecules per cm^3 per s]	$CH_2OH + R \rightarrow H + H_2CO$ [r_{222}; 4.6×10^{-1} molecules per cm^3 per s]
CH_3O		
Formation pathway		
1st reaction	$H + H_2CO \rightarrow CH_3O$ [r_{225}; 2.4×10^{-23} molecules per cm^3 per s]	$H + H_2CO \rightarrow CH_3O$ [r_{225}; 2.4×10^{-23} molecules per cm^3 per s]
2nd reaction	$H + CH_2OO \rightarrow O + CH_3O$ [r_{788}; 5.0×10^{-23} molecules per cm^3 per s]	$H + CH_2OO \rightarrow O + CH_3O$ [r_{788}; 5.0×10^{-23} molecules per cm^3 per s]
Consumption pathway		
1st reaction	$CH_3O + R \rightarrow H + H_2CO$ [r_{224}; 6.7×10^{-1} molecules per cm^3 per s]	$CH_3O + R \rightarrow H + H_2CO$ [r_{224}; 6.7×10^{-1} molecules per cm^3 per s]
2nd reaction	$CH_3O + R \rightarrow H_2 + HCO$ [r_{266}; 4.9×10^{-1} molecules per cm^3 per s]	CH3O + R → H2 + HCO [r_{266}; 4.9×10^{-1} molecules per cm^3 per s]
H_2O_2		
Formation pathway		
1st reaction	$HCOOH + R \rightarrow C + H_2O_2$ [r_{323}; 5.2×10^{-7} molecules per cm^3 per s]	$H + HO_2 \rightarrow H_2O_2$ [r_{105}; 4.5×10^{-23} molecules per cm^3 per s]
2nd reaction	$OH + OH \rightarrow H_2O_2$ [r_{115}; 3.1×10^{-24} molecules per cm^3 per s]	H2 + O2 → H_2O_2 [r_{109}; 4.8×10^{-23} molecules per cm^3 per s]
Consumption pathway		
1st reaction	$H_2O_2 + R \rightarrow O + H_2O$ [r_{112}; 5.7×10^{-1} molecules per cm^3 per s]	$H_2O_2 + R \rightarrow O + H_2O$ [r_{112}; 5.7×10^{-1} molecules per cm^3 per s]
2nd reaction	$H_2O_2 + R \rightarrow H_2 + O_2$ [r_{108}; 5.7×10^{-1} molecules per cm^3 per s]	$H_2O_2 + R \rightarrow H_2 + O_2$ [r_{108}; 5.7×10^{-1} molecules per cm^3 per s]
HOCO		

Table 4 (*Contd.*)

	Low-dose irradiated ice (beginning of experiment) [reaction label; effective reaction rate]	Highly irradiated ice (CE phase) [reaction label and effective reaction rate]
Formation pathway		
1st reaction	HCOOH + R → H + HOCO [r_{234}; 6.9×10^{-24} molecules per cm^3 per s]	H + CO_2 → HOCO [r_{231}; 6.9×10^{-24} molecules per cm^3 per s]
2nd reaction	O + HCOOH → OH + HOCO [r_{1240}; 3.25×10^{-23} molecules per cm^3 per s]	O + HCOOH → OH + HOCO [r_{1240}; 3.25×10^{-23} molecules per cm^3 per s]
Consumption pathway		
1st reaction	HOCO + R → H + CO_2 [r_{230}; 1.7×10^{-2} molecules per cm^3 per s]	H + HOCO → H_2 + CO_2 [r_{763}; 3.2×10^{-23} molecules per cm^3 per s]
2nd reaction	H + HOCO → H_2 + CO_2 [r_{763}; 3.2×10^{-23} molecules per cm^3 per s]	H + HOCO → HCOOH [r_{235}; 2.9×10^{-23} molecules per cm^3 per s]

[a] The remaining reactions can be found in SI 2.

indicating a sequential oxidation mechanism leading to CO_2 and H_2O. These qualitative results agree with previous experimental data on irradiated cold ices: Andrade *et al.*[3] (2013) observed abundant CO and CO_2 in irradiated HCOOH ice, and matrix-isolation studies have documented HOCO as a predominant product.[36] This correspondence strengthens the astrophysical relevance of the identified pathways, suggesting that analogous processes may occur in interstellar icy mantles. Some specific reactions (particularly those involving the generic radical R from dissociation reactions) still lack detailed characterization; such uncertainties are noted in the SI and point to directions for future investigation.

3.4 Comparison with literature data and previous models employing PROCODA

The initial molecular composition of the ice strongly modulates the products observed. For example, in pure formic acid (HCOOH) ice irradiated at 15 K under heavy Fe ions, Andrade *et al.* reported that the most abundant species formed were CO, CO_2, and H_2O.[3] In contrast, in irradiated $H_2O : CO_2$ mixtures, the synthesis of hydrogen peroxide (H_2O_2) and carbon monoxide (the latter containing oxygen originating from water) is observed, particularly when heavier projectiles are employed.[37,38] The presence of molecular O_2 in the ice favors oxidative pathways; indeed, photochemical and radiolytic processing of pure CO_2 and O_2 ices has been shown to lead to the formation of the trioxide carbonate species (CO_3) in such matrices.[37] On the other hand, N_2 acts essentially as a diluent almost inert to ionizing radiation so its inclusion reduces reactive effects without producing significant chemical products (quantitative data for N_2-containing ices remain scarce). In summary, H_2O-rich ices favor ·OH-based pathways (leading, for example, to H_2O_2), whereas CO_2/O_2-rich matrices promote carbon-bearing routes such as CO_3 formation.

The average reactivity parameters and desorption yield also vary with the type of radiation and temperature. In general, heavy and highly energetic ions deposit energy locally much more intensely than lighter particles such as protons or electrons, leading to higher chemical yields.[37] Pilling *et al.*[38] (2011) observed that in $H_2O : CO_2$ ices at 13 K, the effective dissociation cross sections of H_2O and CO_2 were approximately 3–4 times smaller when using ^{16}O ions compared with ^{58}Ni, demonstrating the effect of the projectile's stopping power. The ice temperature plays a decisive role: experiments at ~13 K generally produced much larger quantities of organic compounds than those at 80 K (by a factor of $\gtrsim 4$), indicating that reaction pathways in ultracold ices are more efficient or less thermally suppressed. Regarding irradiation-induced desorption, Andrade *et al.*[3] (2013) estimated yields on the order of 10^5 neutral molecules ejected per Fe-ion impact in HCOOH ice (approximately one charged ion per impact). This high value suggests that neutral-molecule ejection dominates desorption under high-energy irradiation; it is assumed that projectiles with lower deposited energy produce smaller sputtering yields, although direct comparisons with protons or electrons are not available in the literature.[39,40]

Table 5 Comparison of average effective rate coefficients (ERCs) and desorption parameters between the present model and previous PROCODA-based simulations for other astrophysical ices reported in the literature

Average parameter	HCOOH ice at 15 K irradiated by 267 MeV $^{56}Fe^{22+}$ (this work)	N_2 : H_2O ice at 15 K irradiated by 40 MeV Ni^{11+} (L. Queiroz *et al.* 2025)[14]	Pure H_2O ice at 13 K irradiated by 52 MeV Ni $^{11+}$(5)	H_2O : O_2 ice at 9k irradiated by 0.8 MeV H^+ (J. R. C. Silva *et al.* 2025)[15]	Pure H_2O ice at 20 K irradiated by 2 keV electrons (C. H. Da Silveira & S. Pilling 2024)[9]
ERC for radiation-induced dissociation	3.8×10^{-1} s $^{-1}$	3.7×10^{-3} s^{-1}	2.5×10^{-2} s^{-1}	3×10^{-3} s^{-1}	9.6×10^{-2} s^{-1}
ERC for bimolecular collisions	2.3×10^{-23} cm^3 per molecules per s	2.7×10^{-25} cm^3 per molecules per s	4.3×10^{-24} cm^3 per molecules per s	5.3×10^{-25} cm^3 per molecules per s	9.1×10^{-24} cm^3 per molecules per s
ERC for intrinsic desorption	1.36×10^{-3} s^{-1}	5.4×10^{-4} s^{-1}	3.2×10^{-6} s^{-1}	8.3×10^{-9} s^{-1}	1.2×10^{-6} s^{-1}
Desorption rate	8.2×10^{13} molecules per s	6.4×10^{13} molecules per s	1.7×10^{13} molecules per s	1.3×10^{11} molecules per s	9.5×10^{10} molecules per s
Desorption yield	1.5×10^5 molecules per ion	1.2×10^5 molecules per ion	1×10^4 molecules per ion	2.1×10^{-1} molecules per ion	3.2×10^{-4} molecules per electron

Such differences affect the efficiency of formation and destruction routes for key species. For instance, H_2O_2 forms preferentially through recombination of OH radicals generated from H_2O, so its overall formation increases with the water content in the ice.[33] Carbonate species (CO_3), in turn, are formed mainly in CO_2-rich (and O_2-rich) ices: radiolysis of pure CO_2 produces appreciable amounts of CO_3, but this yield decreases drastically when H_2O is incorporated into the system.[4,28,33] In summary, ices with higher H_2O fractions tend to favor oxygen-bearing products such as H_2O_2, whereas those rich in CO_2/O_2 favor carbon-bearing products such as CO_3. These trends, inferred from the referenced experiments, reflect the distinct chemistry of the original constituents.

Table 5 presents the average parameters of effective reaction rate constants (ERC) and desorption yields for different ice systems irradiated under distinct experimental conditions. In general, experiments employing high-energy heavy ions exhibit ERC values for dissociation that are higher than those observed in systems irradiated by protons or electrons, reflecting the greater local energy deposition associated with the stopping power of these projectiles.[2,3] The desorption yields follow the same trend: while each heavy ion can induce the ejection of approximately 10^4 to 10^5 molecules per incident particle, protons typically yield values two to three orders of magnitude lower. Electrons, in turn, show intermediate behavior, with yields in the range of 10^3 to 10^4 molecules per electron.[3] This pattern reflects fundamental differences between interaction mechanisms: heavy ions produce dense ionization tracks, whereas lighter particles deposit energy more diffusely, with lower efficiency in generating sputtering processes.

Among the ice compositions analyzed, several additional trends can be highlighted. Systems containing N_2 exhibit lower ERC values for both dissociation and bimolecular collisions, which can be attributed to the low chemical reactivity of N_2 and its essentially diluting role within the matrix.[3] Conversely, O_2-rich mixtures display reduced collision ERC values, consistent with the observed trend of lower H_2O_2 formation in such matrices.[2] In H_2O : CO_2 mixtures, the effective collision constants are comparatively higher, reflecting the simultaneous participation of radicals derived from water and carbon-bearing species. Furthermore, comparisons among systems reveal that even under cryogenic conditions, the initial ice composition significantly influences the overall efficiency of reaction pathways and the distribution of final products.

These results confirm that the average parameters obtained through the PROCODA modeling approach enable a quantitative correlation between the nature of the projectile, the ice composition, and the efficiency of chemical transformations. The comparative analysis shows that the presence of oxidizing species (such as O_2 or CO_2) can modulate the formation of oxygen-bearing products (such as H_2O_2 or CO_3), whereas inert constituents (such as N_2) tend to reduce reaction efficiency. These patterns are consistent with previously reported experimental studies on the radiolysis of molecular ices.[2,3]

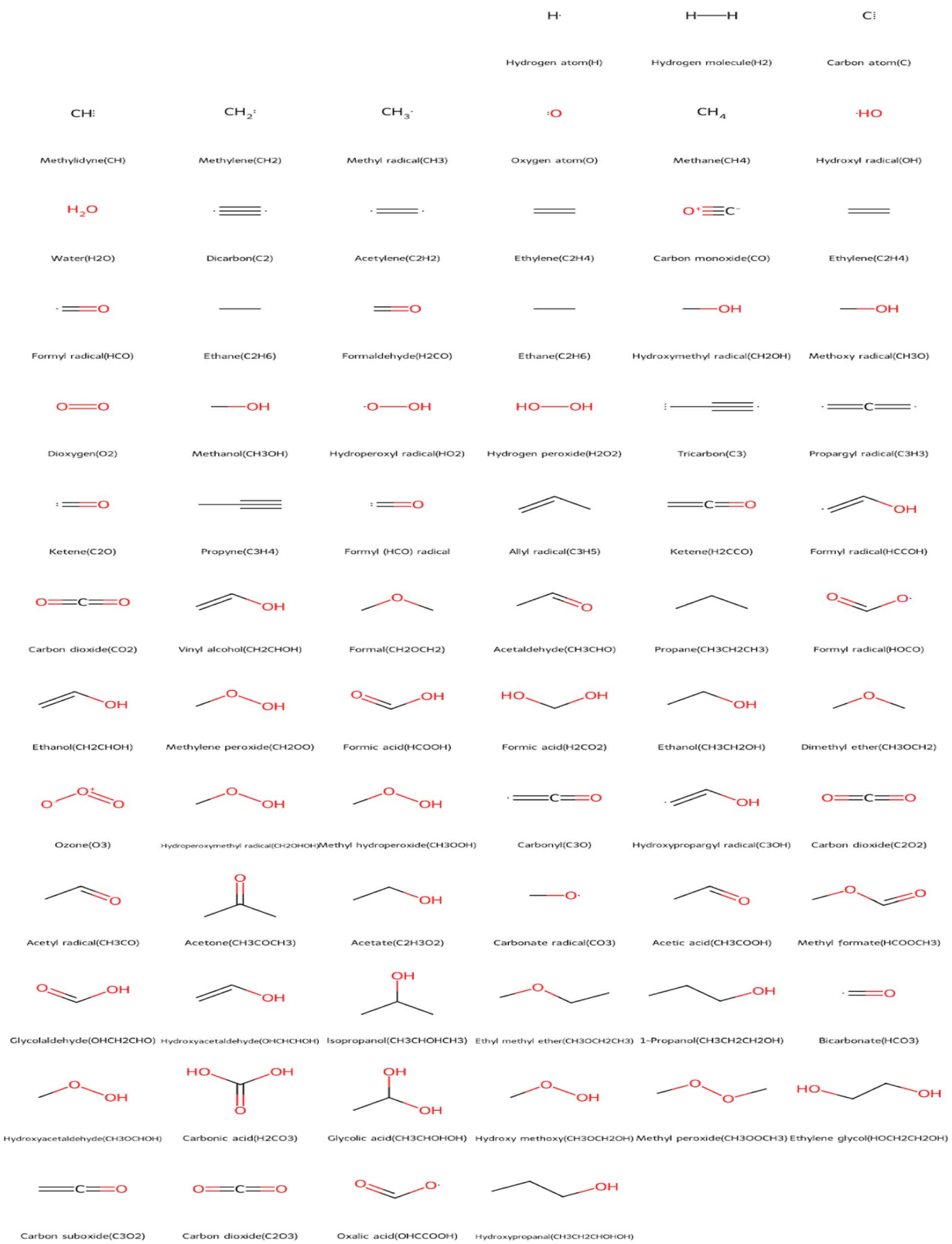

4. Astrophysical implications

Formic acid (HCOOH) is an abundant organic constituent in various cold astrophysical environments. It has been observed in comets, chondritic meteorites, dense dark molecular clouds, and ices in protostellar disks associated with star formation.[1,2] In many of these regions, such as dense clouds and accretion disks, ice grains are shielded from direct stellar ultraviolet radiation, so the chemistry is dominated by high-energy radiation (cosmic rays and photons) that penetrates these environments. Thus, the detection of HCOOH allows us to infer high-energy conditions in the chemical history of these locations.[2,3]

Functionally, HCOOH can act as a precursor molecule for more complex compounds and as a marker of chemical processing. Structurally, formic acid shares elements with glycine, the simplest amino acid, and both serve as models to study prebiotic pathways.[2,3] In laboratory experiments, irradiated HCOOH generates radicals such as HCO and OH, which can recombine to form more complex compounds or revert to HCOOH.[36]

Observations of dense molecular clouds reveal the presence of formic acid in sources such as L134N,[41] as well as in prominent star-forming regions like Orion KL, Sgr B2, Sgr A, and W51.[1,2,22,42–44] In these environments, HCOOH is commonly linked to hot molecules cores and the chemistry associated with massive star formation. Its formation in icy mantles is believed to occur primarily *via* reactions between suprathermal H atoms and CO in H_2O-rich matrices, followed by subsequent processing with OH radicals.[45,46] The results of the present work support this scenario by demonstrating that under heavy-ion irradiation at 15 K, HCOOH is efficiently converted into CO, CO_2, and H_2O, with an effective half-life ($\sim 10^8$ years) consistent with cosmic-ray processing timescales in dense clouds.[3] Therefore, combining these modeled rate coefficients with observational data enables us to constrain the chemical "age" of icy mantles and to infer their irradiation history.

The effective reaction coefficients (ERCs) obtained in this study provide direct input for astrochemical models simulating radiation-driven chemistry in cold ices. Standard gas-phase or surface databases often lack parameters valid under cryogenic and high-energy conditions. Incorporating the ERCs determined here can improve predictions of HCOOH destruction rates, CO and CO_2 production, and the yields of volatile species released by sputtering or desorption. Applying these coefficients to time-dependent astrochemical codes may refine abundance predictions for formic acid and its radiolytic products in environments where cosmic-ray ionization dominates the energy budget (*e.g.*, dense cloud cores and outer disk midplanes).[26,27]

From an observational perspective, the model results can guide future telescope searches for formic acid and related species in cold regions. Promising targets include dark clouds such as TMC-1 and L134N, protostellar envelopes below 20 K, and outer Solar System objects with mixed H_2O : CO ices (*e.g.*, Europa, Ganymede). Measuring the HCOOH/CO_2 or HCOOH/CO ratio in these environments may help diagnose the extent of cosmic-ray processing or irradiation fluence. Facilities such as JWST and ALMA through infrared and millimeter spectroscopy can potentially resolve the weak vibrational and rotational bands of HCOOH and constrain its spatial distribution within these ices.[47]

In environments such as icy moons, where H_2O and CO coexist under strong magnetic and cosmic-ray bombardment, irradiated HCOOH is expected to reach detectable levels.[2] Consequently, formic acid acts both as a chemical tracer of energetic processing and as a potential prebiotic precursor in planetary and interstellar settings. Its radiolytic degradation mainly produces CO, CO_2, and H_2O, whose spectral signatures remain key diagnostics for assessing the chemical state and irradiation history of cold astrophysical ices.[2,3]

5. Conclusion

This study revisited the chemical evolution of pure formic acid (HCOOH) ice irradiated at 15 K by heavy, highly charged cosmic-ray analogs ($^{56}Fe^{22+}$, 267 MeV), based on the experimental dataset of Andrade *et al.*[3] (2013). The kinetic modeling performed with the PROCODA code incorporated 73 chemical species coupled through 1631 reactions, including dissociation, recombination, oxidation, and desorption processes. The results provide a quantitative and mechanistic interpretation of HCOOH radiolysis under astrophysically relevant conditions. Our main conclusions are:

(i) Kinetic modeling: the PROCODA simulation reproduced the chemical evolution of observed species in the experiment (HCOOH, CO, CO_2, and H_2O) and also map the evolution of other 69 species expected to exist in the irradiated ice (including radicals and intermediates) that were inaccessible to spectroscopy, accurately describing the balance between molecular destruction and recombination and the steady-state composition of irradiated HCOOH ice.

(ii) Chemical equilibrium and relevant species: at high fluence, the system reached a dynamic equilibrium dominated by CO_2, CO, and H_2O, with transient HOCO and OH radicals mediating oxidation and molecular regeneration, consistent with previous laboratory observations. The current model calculates abundances in this phase that is also inaccessible to spectroscopy data.

(iii) Desorption behavior: radiation-induced desorption yielded $\sim 10^5$ neutral molecules per incident ion, in agreement with experimental data, indicating that energetic particle impacts significantly enhance gas–ice exchange in dense molecular environments.

(iv) Dominant reaction pathways: the main formation route of HCOOH is H + HOCO → HCOOH, while its destruction proceeds primarily *via* O + HCOOH → OH + HOCO and H + HCO → H_2 + CO, confirming hydrogen abstraction and oxidation as key low-temperature mechanisms in carboxylic acid chemistry.

(v) Astrophysical relevance: the derived effective reaction coefficients (ERCs) are suitable for incorporation into astrochemical databases and models of cold environments exposed to ionized radiation (*e.g.*, comets, dense clouds, protoplanetary disks, icy moons). The model points to promising targets for

future JWST and ALMA observations, providing an observational framework to assess the modeled chemistry in astrophysical ices.

In summary, the present work quantitatively links laboratory radiolysis of formic acid to reaction kinetics and astrochemical observables. By coupling experimental data with the PROCODA modeling framework, this study advances the understanding of radiation-driven reaction networks in cryogenic ices, bridging the disciplines of physical chemistry and astrochemistry. The resulting reaction coefficients and mechanistic insights provide a robust foundation for interpreting the chemical evolution of icy grains in molecular clouds and for refining models of organic molecule formation in the interstellar medium.

Within this context, PROCODA should be regarded as a macrokinetic tool aimed at reproducing experimentally observable trends and steady-state chemical behavior in irradiated ices, rather than a detailed description of the primary electronic or ionic processes underlying radiation chemistry.

Conflicts of interest

The authors declare that they have no known competing financial interests or personal relationships that could have appeared to influence the work reported in this paper.

Data availability

The data underlying this article will be shared on reasonable request to the corresponding author.

Appendix A1 – the 73 employed chemical species in the model

The species considered in the model (observed and expected) were:

Acknowledgements

The authors acknowledge the Brazilian research agencies Conselho Nacional de Desenvolvimento Científico e Tecnológico – CNPq (projects #302985/2018-2; #302608/2022-2 and #130352/2024-1) and Fundação de Amparo à Pesquisa do Estado de São Paulo – FAPESP (project #2024/05115-5).

References

1 H. M. Boechat-Roberty, S. Pilling and A. C. F. Santos, Destruction of formic acid by soft X-rays in star-forming regions, *Astron. Astrophys.*, 2005, **438**(3), 915–922.
2 S. Pilling, A. C. F. Santos and H. M. Boechat-Roberty, Photodissociation of organic molecules in star-forming regions – II. Acetic acid, *Astron. Astrophys.*, 2006, **449**(3), 1289–1296.
3 D. P. P. Andrade, A. L. F. de Barros, S. Pilling, A. Domaracka, H. Rothard, P. Boduch and E. F. Da Silveira, Chemical reactions induced in frozen formic acid by heavy ion cosmic rays, *Mon. Not. R. Astron. Soc.*, 2013, **430**(2), 787–796.
4 S. Pilling, *et al.*, Ion-induced chemistry in complex ice mixtures under astrophysical conditions, *Astrophys. J.*, 2022, **925**, 147.
5 S. Pilling, *et al.*, Radiation-driven chemistry of mixed ices: linking laboratory and astrochemical modeling, *Mon. Not. R. Astron. Soc.*, 2023, **523**, 2858.
6 S. Pilling, *et al.*, Radiolytic processing of astrophysical ice analogs: new insights from laboratory experiments, *Astrophys. J.*, 2023, **952**, 17.
7 S. Pilling, M. S. Mateus, A. Ojeda-González, L. F. A. Ferrão, B. R. L. Galvão, P. Boduch and H. Rothard, Influence of temperature on the chemical evolution and desorption of pure CO ices irradiated by cosmic-rays analogues, *Mon. Not. R. Astron. Soc.*, 2024, **528**(4), 6075–6098.
8 S. Pilling, *et al.*, Heavy-ion induced chemistry in astrophysical ices: towards realistic cosmic ray simulations, *Adv. Space Res.*, 2023, **71**, 5466.
9 C. H. Da Silveira and S. Pilling, Modeling the chemical evolution and kinetics of pure H2O ices under various types of radiation employing the PROCODA code, *Adv. Space Res.*, 2024, **73**(1), 1149–1169.
10 S. Gerasimenko, G. A. Carvalho, F. Zanatto, F. K. Santana and S. Pilling, Characterization of the chemical evolution of CH4 ices under processing by cosmic ray analogues with the PROCODA code–I: Effective reaction rate coefficients and chemical equilibrium phase, *Mon. Not. R. Astron. Soc.*, 2025, **544**(1), 855–865.
11 F. Zanatto, *et al.*, CHn chemical reaction pathways from cosmic ray irradiation of CH4 ices, *J. Chem. Theory Comput.*, 2025, submitted for publication.
12 A. P. A. Carvalho, S. Pilling and A. Domaracka, Radiolysis and desorption processes in astrophysical ices induced by swift ions, *Mon. Not. R. Astron. Soc.*, 2022, **510**, 5170.
13 G. A. Carvalho, S. Pilling and S. Gerasimenko, Characterization of acetonitrile ice irradiated by X-rays employing the PROCODA code–II: Desorption processes, *Mon. Not. R. Astron. Soc.*, 2024, **527**(2), 2781–2789.
14 L. M. S. V. Queiroz, J. R. C. Silva, L. F. A. Ferrão and S. Pilling, Characterization of H2O:N2 ice under bombardment by cosmic rays–I: Reaction rates and chemical equilibrium, *Mon. Not. R. Astron. Soc.*, 2025, **537**(4), 3100–3108.
15 J. R. C. Silva, L. M. S. V. Queiroz, L. F. A. Ferrão and S. Pilling, Molecular evolution of H2O:O2 ices at different temperatures in simulated space environments. I. Chemical kinetics and equilibrium, *Astrophys. J.*, 2025, **985**(2), 254.
16 J. R. C. Silva, *et al.*, Molecular evolution of H2O:O2 ices at different temperatures in simulated space environments – Part 2: Evolution of reaction pathways, *Astrophys. J.*, 2025, **985**, 254.
17 L. Moraes and S. Pilling, Modeling the chemical evolution of cosmic-ray irradiated H_2O:CO_2 ices with PROCODA: Implications for protostars and trans-Neptunian objects, *Icarus*, 2025, submitted for publication.
18 C. M. F. Fargnoli, L. Moraes and S. Pilling, Modeling radiolysis in H_2O:HCOOH ices to connect laboratory

experiments with astronomical spectra, *Planet. Space Sci.*, 2025, submitted for publication.
19 S. Pilling, *et al.*, Radiation-induced chemistry in CO:CO_2 ices: Part 1 – Reaction kinetics and equilibrium abundances, *Adv. Space Res.*, 2025, DOI: 10.1016/j.asr.2026.02.056.
20 C. J. Bennett, C. S. Jamieson, A. M. Mebel and R. I. Kaiser, Reaction dynamics of formic acid formation in astrophysical ices, *Astrophys. J.*, 2011, **727**, 27.
21 A. Bergantini, S. Pilling, F. D. Nunes and H. M. Boechat-Roberty, Irradiation of formic acid-containing ices: laboratory simulations, *Mon. Not. R. Astron. Soc.*, 2014, **437**, 2723.
22 S. Y. Liu, D. M. Mehringer and L. E. Snyder, Interstellar detection of formic acid and related species, *Astrophys. J.*, 2001, **552**, 654.
23 N. Biver, *et al.*, Ethyl alcohol and sugar in comet Lovejoy, *Sci. Adv.*, 2015, **1**, e1500863.
24 R. Basalgète, D. Torres-Díaz, A. Lafosse, L. Amiaud, L. Philippe, X. Michaut, J. H. Fillion and M. Bertin, X-ray photodesorption of complex organic molecules in protoplanetary disks, *Astron. Astrophys.*, 2025, **701**, A251.
25 H. Chaabouni, S. Baouche, S. Diana and M. Minissale, Surface chemistry of interstellar ices under UV irradiation, *Astron. Astrophys.*, 2020, **636**, A4.
26 T. J. Millar, C. Walsh, M. Van de Sande and A. J. Markwick, The UMIST database for astrochemistry 2022, *Astron. Astrophys.*, 2024, **682**, A109.
27 V. Wakelam, P. Gratier, J. C. Loison, K. M. Hickson, J. Penguen and A. Mechineau, The 2024 KIDA network for interstellar chemistry, *Astron. Astrophys.*, 2024, **689**, A63.
28 E. Seperuelo Duarte, A. Domaracka, H. Rothard, P. Boduch and E. F. Da Silveira, Laboratory simulation of cosmic ray induced chemistry in astrophysical ices, *Astron. Astrophys.*, 2010, **512**, A71.
29 M. H. Moore and R. L. Hudson, IR spectra and radiation chemistry of ices relevant to comets, *Icarus*, 2000, **145**, 282.
30 Y. J. Chen, A. Ciaravella, G. M. Caro, C. Cecchi-Pestellini, A. Jiménez-Escobar, K. J. Juang and T. S. Yih, Soft X-ray irradiation of methanol ice: formation of products as a function of photon energy, *Astrophys. J.*, 2013, **778**(2), 162.
31 F. Schmidt, T. Borrmann, M. P. Mues, S. Benter, P. Swiderek and J. H. Bredehöft, Mechanisms of electron-induced chemistry in molecular ices, *Atoms*, 2022, **10**(1), 25.
32 F. A. Vasconcelos, S. Pilling, W. R. M. Rocha, H. Rothard and P. Boduch, Radiolysis of N2-rich astrophysical ice by swift oxygen ions: implication for space weathering of outer solar system bodies, *Phys. Chem. Chem. Phys.*, 2017, **19**(35), 24154–24165.
33 E. Dartois, B. Augé, H. Rothard, *et al.*, Ion-induced chemistry in ices: track effects and molecular processing, *Nucl. Instrum. Methods Phys. Res., Sect. B*, 2015, **365**, 472–476.
34 K. I. Öberg, V. V. Guzmán, C. Walsh, *et al.*, The molecular inventory of protoplanetary disks, *Astrophys. J., Suppl. Ser.*, 2021, **257**, 1.
35 B. Lefloch, C. Ceccarelli, C. Codella, C. Favre, L. Podio, C. Vastel, S. Viti and R. Bachiller, The chemical complexity of solar-type protostars, *Mon. Not. R. Astron. Soc.*, 2017, **470**, 169–178.
36 S. V. Ryazantsev and V. I. Feldman, Radiation-induced transformations of matrix-isolated formic acid: evidence for the HCOOH → HOCO + H channel, *Phys. Chem. Chem. Phys.*, 2015, **17**(45), 30648–30658.
37 S. Pilling, E. S. Duarte, A. Domaracka, H. Rothard, P. Boduch and E. F. Da Silveira, Radiolysis of H_2O:CO_2 ices by heavy energetic cosmic ray analogs, *Astron. Astrophys.*, 2010, **523**, A77.
38 S. Pilling, E. S. Duarte, A. Domaracka, H. Rothard, P. Boduch and E. F. Da Silveira, Radiolysis of astrophysical ice analogs by energetic ions: the effect of projectile mass and ice temperature, *Phys. Chem. Chem. Phys.*, 2011, **13**(35), 15755–15765.
39 A. Bergantini, S. Pilling, H. Rothard, P. Boduch and D. P. P. Andrade, Processing of formic acid-containing ice by heavy and energetic cosmic ray analogues, *Mon. Not. R. Astron. Soc.*, 2014, **437**(3), 2720–2727.
40 C. J. Bennett, T. Hama, Y. S. Kim, M. Kawasaki and R. I. Kaiser, Laboratory studies on the formation of formic acid (HCOOH) in interstellar and cometary ices, *Astrophys. J.*, 2010, **727**(1), 27.
41 V. Lattanzi, A. Walters, B. J. Drouin and J. C. Pearson, Submillimeter spectrum of formic acid, *Astrophys. J., Suppl. Ser.*, 2008, **176**(2), 536.
42 S. Y. Liu, J. M. Girart, A. Remijan and L. E. Snyder, Formic acid in Orion KL from 1 millimeter observations with the Berkeley-Illinois-Maryland Association Array, *Astrophys. J.*, 2002, **576**(1), 255.
43 Y. C. Minh, W. M. Irvine and P. Friberg, Molecular abundances in the Sagittarius A molecular cloud, *Astron. Astrophys.*, 1992, **258**, 489–494.
44 G. Winnewisser and E. Churchwell, Detection of formic acid in Sagittarius B2 by its transition, *Astrophys. J.*, 1975, **200**, L33–L36.
45 R. T. Garrod and E. Herbst, Formation of methyl formate and other organic species in the warm-up phase of hot molecular cores, *Astron. Astrophys.*, 2006, **457**(3), 927–936.
46 S. Ioppolo, H. M. Cuppen, E. F. Van Dishoeck and H. Linnartz, Surface formation of HCOOH at low temperature, *Mon. Not. R. Astron. Soc.*, 2011, **410**(2), 1089–1095.
47 A. A. Boogert, P. A. Gerakines and D. C. B. Whittet, Observations of the icy universe, *Annu. Rev. Astron. Astrophys.*, 2015, **53**(1), 541–581.